JOURNAL OF MATERIALS SCIENCE 14 (1979) 2865–2871

Natural carbonate-reinforced composite materials

Part 1 *Morphology of sea urchin teeth*

W. BONFIELD
Department of Materials, Queen Mary College, London E1 4NS, UK

M. SCANDOLA
Centro di Studio per la Fisica delle Macromolecole del CNR, Bologna, Italy

A scanning electron microscopy study of the structure of teeth from the sea urchin *Echinus esculentus* revealed a variety of crystalline plates, discs and fibres. Two composite-like regions reinforced with aligned fibres were identified, one in the central "stone-part", with a particulate matrix, and the other, with interconnecting discs, in the keel of the tooth. Microprobe analysis established the presence of Mg and Ca, with a variable Mg/Ca ratio, which was attributed to the composition $Ca_xMg_yCO_3$.

1. Introduction

The assembly of two or more constituents to form a reinforced composite structure is a feature of the skeletal materials in most animal species. As a general example, compact bone in vertebrates consists of relatively small (~5 nm × 60 nm × 60 nm), plate-like particles of hydroxyapatite ($Ca_{10}(PO_4)_6(OH)_2$), distributed in a continuous collagen matrix.

There are also some natural composite materials in which the reinforcing phase exists as carbonate in the form of calcite ($CaCO_3$) or dolomite ($Ca_{0.5}Mg_{0.5}CO_3$). Recently, Brear and Currey [1] commented on the composite-like structure of the central region of a tooth of the sea urchin *Psammechinus milaris* in which, it was suggested, single crystals of calcite were regularly packed in an amorphous and only partially complete matrix. The important feature of this structure is the scale of the reinforcing crystals (~10 μm in cross-sectional diameter and several mm in length), which would facilitate its study as an example of a natural composite material. This paper reports on the morphology of another, and larger, sea urchin tooth (*Echinus esculentus*), as a prelude to a determination of its associated mechanical properties and the development of a composite model. Although this tooth has not been studied previously, Märkel and his associates, in a comprehensive series of papers [2–7] have discussed the structure of various sea-urchin teeth and identified an assembly of calcite or dolomite fibres, plates, prisms and discs. For consistency, the terminology developed by Märkel is continued and the results are considered in terms of his structural concepts, with particular emphasis on the evaluation of composite-like regions.

2. Experimental method

The five teeth of *Echinus esculentus* are contained in a structure designated as Aristotle's lantern, as shown in Fig. 1. The teeth are ~30 mm in length, with ~5 mm external to the lantern and have a curved profile with a characteristic T-shaped cross-section. Samples of teeth, loosened and removed from the lantern by maceration in 5% KOH, were fractured by manual bending and the approximately transverse fracture surfaces were examined in a JEOL-JX50A scanning electron probe micro-analyser. Some fracture surfaces were also mechanically polished for an assessment of the Mg/Ca ratio.

3. Results

3.1. Scanning microscopy

The external appearance of the scaping end of a

0022–2461/79/122865–07$02.70/0

Figure 1 (a) Arrangement of five teeth in Aristotle's lantern shown end-on and side-view and (b) a separated tooth (1 scale division = 1 mm).

tooth is shown in Fig. 2 and illustrates both the essentially T-shaped cross-section of the shaft (with a "wedge" stiffened by a "keel") and the worn tip. Fracturing the tooth by manual bending at about its mid-point produced the two complementary fracture surfaces shown in Fig. 3, from which, at this level of magnification, the main internal components of structure can be identified as:

(a) A wedge shape composed of two sets of parallel plates, mutually perpendicular and disposed symmetrically at $\sim 45^{\circ}$ to the central axis of the tooth, which are referred to as the primary and secondary plates.

(b) A central "featureless" region within the wedge, which extends vertically to the tip of the tooth.

(c) Coarse fibres aligned along the length of the

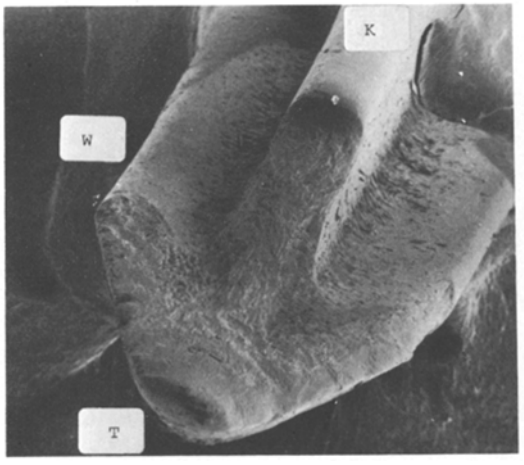

Figure 2 Scraping tip (T), illustrating the wedge (W) and stiffening keel (K). Note evidence of wear extending from the leading edge (× 25).

tooth in the keel section, enclosed by other plates (the keel or carinar appendages).

These features are considered in turn at higher magnification. Fig. 4 shows the termination of parallel primary plates to form the flat top surface or crust of the tooth. It can be seen that the rows of holes on the external crust follow the edges of the primary plates. Irregularly shaped discs separate each primary plate as shown in Fig. 4 and, in more detail, in Fig. 5. Towards the central axis the primary plates diverge from a 45° orientation, an effect which increases the plate separation (Fig. 6). At a greater depth from the surface, the primary plates are curved and appear continuous across the central axis. Fig. 6 also shows the secondary plates which form at ~90° to the primary plates. It can be seen that these plates are shorter, more irregular and more separated than the primary plates.

The primary and secondary plates partially surround the central region of the wedge, referred to as the stone-part, which emerges to form the tip of the tooth and is used to graze algae from rocks. The stone-part is shown in Fig. 7, which demonstrates a structure of aligned fibres, with an approximately circular cross-section (~2 μm in diameter). It can be seen that each fibre is partially or completely covered with a particulate surface deposit (up to ~1 μm in thickness), which is bonded (either partially or completely) to adjacent fibre coatings and constitutes a continuous matrix phase.

Each secondary plate connects with a carinar appendage which encloses the fibres in the centre of the keel of the tooth (Fig. 8). These fibres, which are generally aligned along the length of the tooth, have a circular or ellipsoidal cross-section (~20 μm in diameter). The fibres are not covered with a surface deposit, but are in contact through irregularly spaced disc-shaped plates.

The shaft of the tooth is secured to the lantern by pillar bridges such as shown in Fig. 9a. These pillar bridges are connected to the jaw by col-

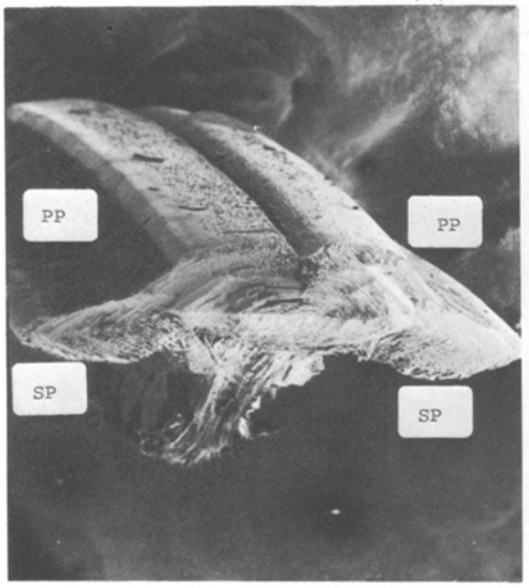

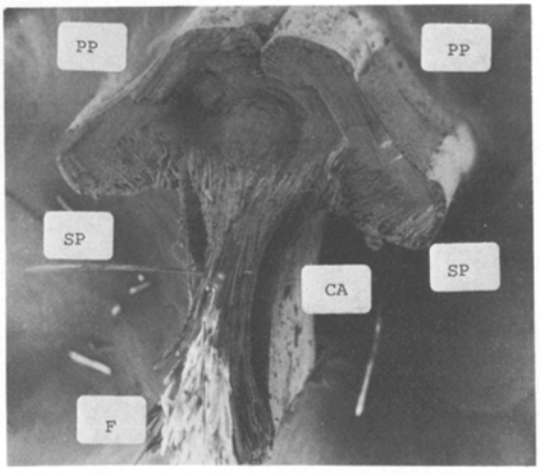

Figure 3 Complementary fracture surfaces obtained by manual bending, showing primary prisms (PP), secondary prisms (SP), fibres (F) and carinar appendages (CA) (× 30).

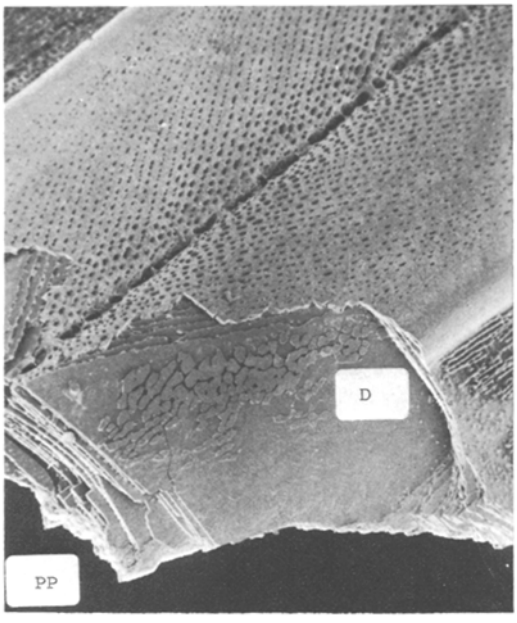

Figure 4 Intersection of primary prisms (PP) with surface crust and separating discs (D) (× 75).

lageous fibrils, which can be readily seen in non-chemically extracted teeth (Fig. 9b).

3.2. Microprobe analysis

The characteristic X-radiations for Ca and Mg were measured during constant rate traverses of polished sections. The measured count is a function of the element concentration and also the packing density of the structure. This latter effect is demonstrated in Fig. 10, in a traverse from the secondary plates to the primary plates. It can be

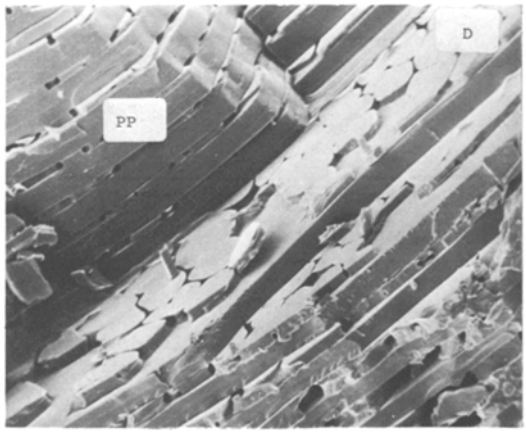

Figure 5 Primary prisms (PP) and separating discs (D) (× 60).

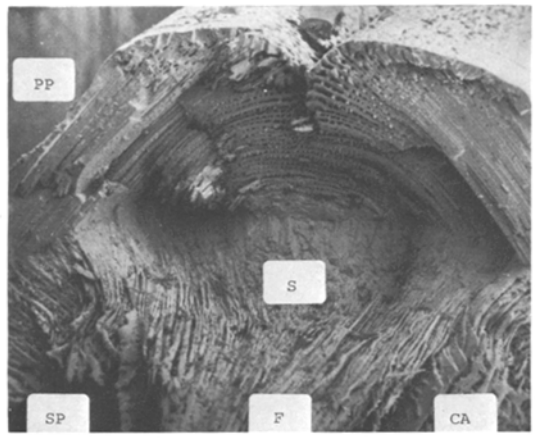

Figure 6 Assembly of primary prisms (PP) and secondary prisms (SP), carinar appendages (CA), central stone-part (S) and keel fibres (F) (× 60).

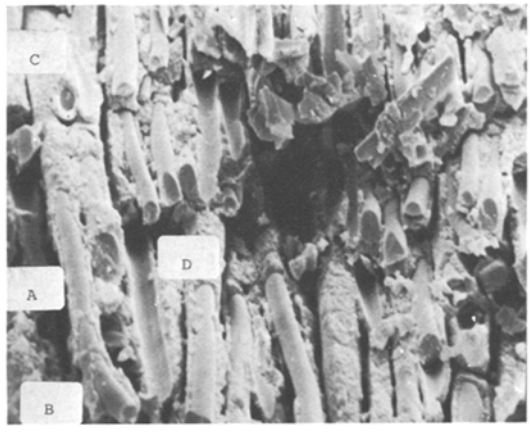

Figure 7 Fibres in the stone-part with partial or complete surface coatings, with examples of fibre debonding (A), fibre pull-out (B), fibre fracture without pull-out (C) and coatings with fibres (D) (× 1900).

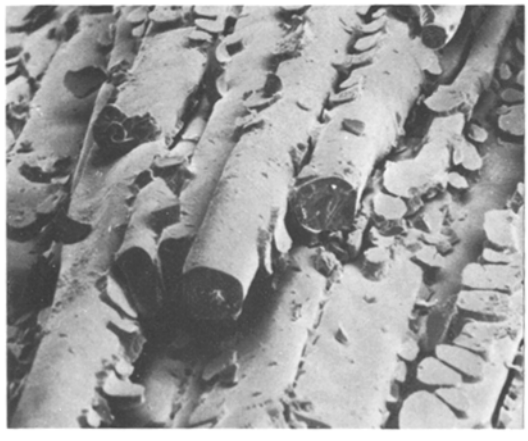

Figure 8 Regularly packed fibres in the keel separated with intermediate discs (× 660).

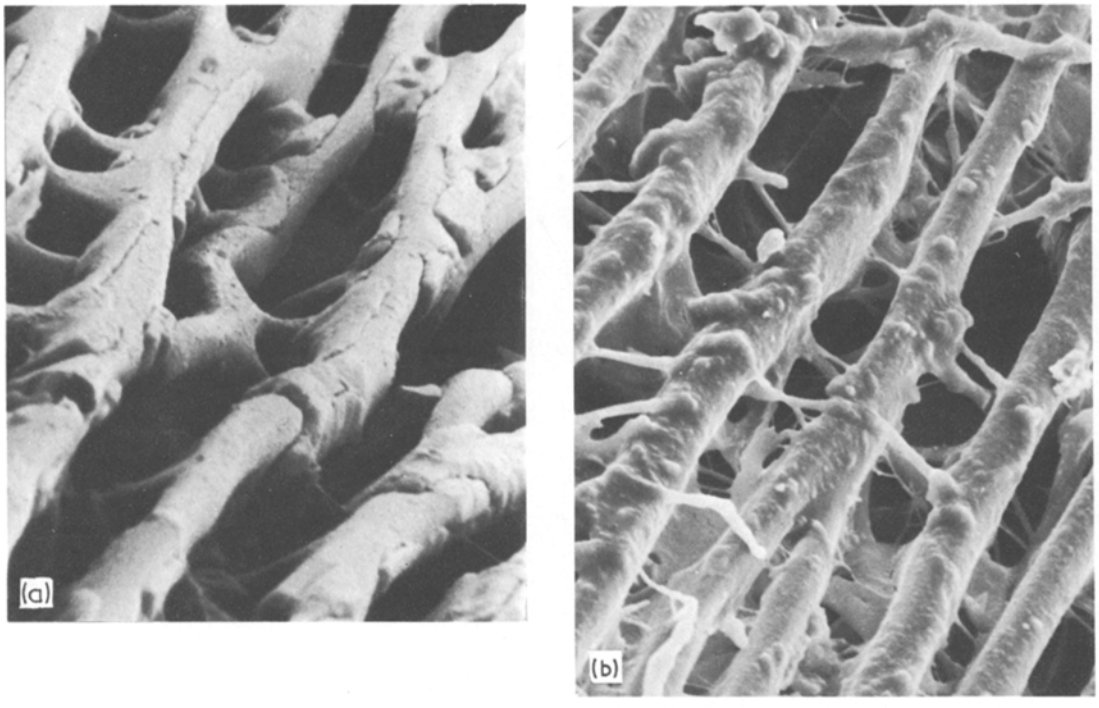

Figure 9 Pillar bridges connecting the tooth to the jaw (a) after maceration (X 2300), (b) without maceration (X 1800), showing collageneous fibrils.

seen that both MgKα and CaKα counts increase towards the denser central region at the primary/secondary plate interface. In fact, the ratio of the counts for MgKα and CaKα in the prism regions remains approximately constant across the section (MgKα/CaKα ~ 0.10).

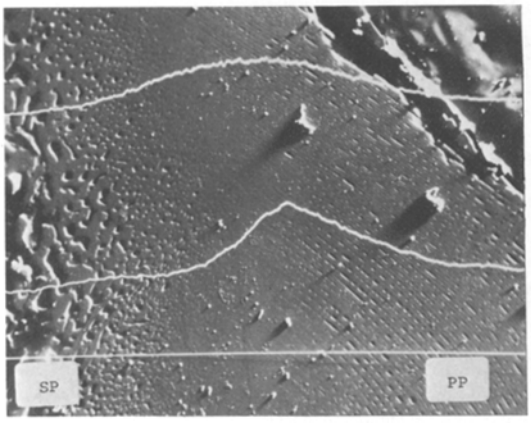

Figure 10 CaKα (upper trace) and MgKα (lower trace) profiles obtained during a microprobe analysis along the marked line from the secondary prisms (SP) to the primary prisms (PP) (X-ray counts: CaKα ~ 2000 minimum, ~ 12 000 maximum, MgKα ~ 500 minimum, ~ 1200 maximum) (X 25).

However, a traverse across the stone-part of the structure reveals a significant variation in the MgKα/CaKα ratio. Figs. 11a and b show the counts for MgKα and CaKα, respectively, recorded in a traverse from the keel across the stone-part to the primary prisms. It can be seen that, both Ca and Mg are present in the keel, stone-part and primary prisms, but that the CaKα profile shows a broad maximum in the centre of the stone-part, while the MgKα profile exhibits a narrow maximum at the interface of the stone-part and the primary prisms, and a significant decrease across the stone-part to the interface with the keel, with MgKα/CaKα decreasing from ~ 0.28 to ~ 0.10. It was not possible in these scans to distinguish between the crystalline fibres and the particulate coatings (matrix).

4. Discussion

The macroscopic and microstructural observations and microprobe analysis reveal several levels of functional morphology. At a macroscopic level, the scraping wedge is stiffened by a keel and this external shape is achieved by regular arrangements of plates and discs. At a microscopic level, the plates and discs are seen to surround two re-

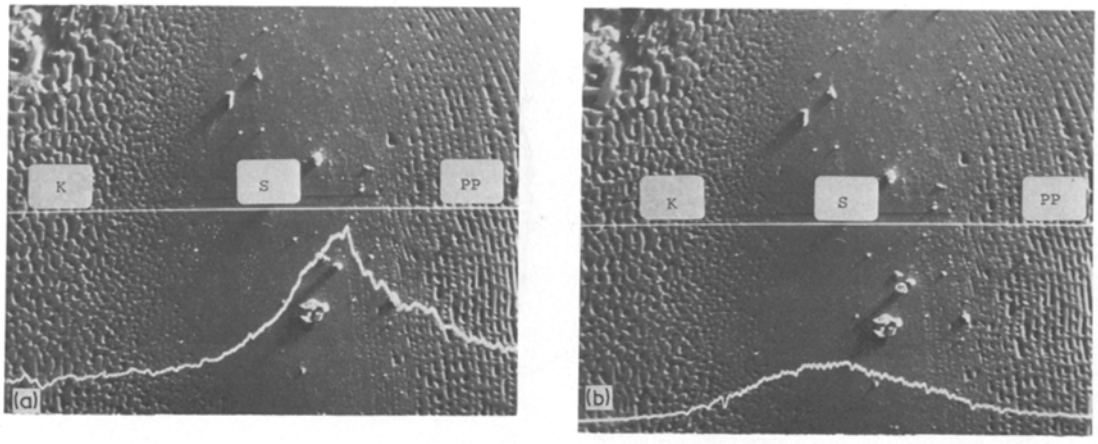

Figure 11 MgKα (a) and CaKα (b) profiles obtained during microprobe analysis along the marked line, from the keel (K) across the stone-part (S) to the primary prisms (PP). (X-ray counts: CaKα ~ 400 minimum ~ 10 000 maximum, MgKα ~ 400 minimum ~ 2200 maximum) (× 30).

inforced composite structures, namely the stone-part and the central region of the keel.

It should be emphasised the stone-part surface (Fig. 7) was prepared by a fracture process, which has modified the structure. It is suggested that fibre debonding and "pull-out" by interfacial shearing have accompanied the propagation of cracks through the surface coatings which constitute the matrix phase. In contrast, with the absence of an extensive matrix phase, and only localized "keying" by discs, no fibre debonding or pull-out were observed in the keel fracture surface.

Some preliminary deductions as to the nature of the fracture process in the stone-part can be made from Fig. 7. It can be seen that most of the fibres exhibit some debonding from the matrix (i.e. the fibre is only partially coated). As the fracture surface is not a continuous plane, it is difficult to establish the extent of fibre pull-out, but if it is assumed that pull-out is indicated by any length of fibre extending from the *fibre* fracture surface which is completely devoid of coating, then most fibres also show some pull-out. This effect is also demonstrated by several examples of coatings without fibres (which presumably remained on the complementary fracture surface). For a few fibres, fracture occurred without debonding or pull-out. These observations indicate that most fibres exceeded the critical length (l_c) required to achieve a maximum "plateau" stress [8] (i.e. are essentially similar to a continuous composite with infinitely long fibres) and during fracture the interfacial shear stress developed at the fibre-coating interface was sufficient to produce debonding and pull-out. For other fibres, with a length less than the critical length, the interfacial shear stress at fracture was smaller and not sufficient to produce debonding and pull-out.

The mean length of fibre pull-out ($\bar{l}_p$) is generally assumed (e.g. [8]) to be half of the maximum possible pull-out length ($l_{p\,max}$).

We have

$$l_{p\,max} = \frac{l_c}{2} \tag{1}$$

and hence

$$\bar{l}_p \simeq \frac{l_c}{4} \tag{2}$$

From Fig. 7, $\bar{l}_p$ is ~ 4 μm and therefore l_c is ~ 16 μm.

Alternatively, it is often assumed that the maximum debond length (l_b) is of the order of l_c. From Fig. 7, l_b, and hence l_c, is ~ 18 μm. Hence reasonable agreement is obtained between the two derived values of l_c. With an average fibre "diameter" (d) of ~ 2 μm, we obtain a critical aspect ratio, l_c/d of ~ 8.5.

All the fibres in the stone-part and keel exhibited fracture on a characteristic cleavage plane. There is no evidence of necking or inter-crystalline fracture and it is concluded that the fibres are brittle single crystals. This agrees with the general understanding that skeletal elements in echinoderms are single crystals [9].

It is interesting to note that the stone-part, which emerges as the working tip of the tooth is, as judged from the structural standpoint, stronger (and stiffer) than the centre of keel, as it contains smaller diameter rods, (i.e. a higher packing

volume fraction is obtained) with matrix bonding. This suggestion was confirmed by micro-hardness tests which gave values of 400 to 430 $kg\,mm^{-2}$ in the stone-part and 215 to 235 $kg\,mm^{-2}$ in the centre of the keel. (These values compare with measurements of 300 $kg\,mm^{-2}$ (stone-part) and 186 $kg\,mm^{-2}$ (keel part) made [6] on a tooth of the species *Sphaerechinus granularis*).

At an atomic level, it is apparent that Mg and Ca exist together in the structure, with variations in the Mg/Ca ratio. Previous X-ray diffraction work [10] on sea urchin teeth of *Lytechinus variegatus* has associated Mg entirely with $MgCO_3$ and Ca with $CaCO_3$, with the two carbonates in a solid solution dolomite, $Ca_xMg_yCO_3$. In this previous study, calibration with a standard dolomite sample enabled the count measurements to be converted to mol% of carbonate (although correction was not made for the difference in density between the standard and test specimens). A horizontal traverse (i.e. across the stone-part from primary prism to primary prism) showed a variation from 28.5 to 43.5 (mid-point) to 35.3 mol% $MgCO_3$, while lower levels (to 3.0 mol% $MgCO_3$) were determined in other, unspecified regions of the tooth. With these data, it is reasonable to conclude that the composition of *Echinus esculentus* is also a dolomite, $Ca_xMg_yCO_3$, where x and y can vary. However in contrast to the previous work, the maximum of y was detected at or near the stone-part–primary prism interface. This location emerges as the leading edge of the scraping tip and a decrease in hardness towards the trailing edge (and hence more wear) would correspond to the profile noted in Fig. 2 (and provide the tooth with a self sharpening mechanism).

Acknowledgements

The supply of specimens by Professor J. Currey, University of York, and subsequent helpful discussions are gratefully acknowledged. This research was completed while M.S. was a Research Visitor at Queen Mary College.

References

1. J. D. CURREY and K. BREAR, *J. Mater. Sci.* **11** (1976) 1977.
2. K. MÄRKEL and H. TITSCHACK, *Z. Morph. Tiere* **64** (1969) 179.
3. K. MÄRKEL, *ibid.* **66** (1969) 1.
4. *Idem, ibid.* **68** (1970) 370.
5. *Idem, Ann. Zoo. Jap.* **43** (1970) 188.
6. K. MÄRKEL and P. GORNY, *Z. Morph. Tiere* **75** (1975) 223.
7. K. MÄRKEL, *ibid.* 78 (1974) 221.
8. B. HARRIS, J. MORLEY and D. C. PHILLIPS, *J. Mater. Sci.* **12** (1975) 2050.
9. J.BINYON, "Physiology of Echinoderms" (Pergamon Press, Oxford, 1972).
10. J. H. SCHROEDER, E. J. DWORNIK and J. J. PAPIKE, *Geol. Soc. Amer. Bull.* 80 (1969) 1636.

Received 15 March and accepted 2 April 1979.